Final Assignment - Projects in Data Science [BSPRDAS1KU] - GroupIT

Aniela Marta Ciecierska
anci@itu.dk
Jakub Piotr Gąsior
jaga@itu.dk
Michaela Macejovska
mimac@itu.dk

Francisco Gonçalves Medeiros Lemos Moreno
fmor@itu.dk
Jonas Drøivoldsmo Lesund
jles@itu.dl

Abstract

This paper showcases the route that the members of the group G took in order to explore the capabilities of a machine to identify melanoma, as well as their findings, through different programming algorithms and human evaluations. It contains a description of the process, auxiliary graphs and a conclusion of the results found.

1 Introduction

Artificial intelligence is becoming an undeniable force in technological advancements. Its true capacity is yet to be comprehended, and for this reason, people disagree on what it can or cannot do, as well as what it should or should not do. One of the fields where AI might become a usual tool is medicine. This report will focus on its possible presence in this field, more specifically for detection and diagnosis of melanoma. Melanoma is a form of skin cancer that develops from melanocytes, a type of skin cells. It occurs when these cells grow uncontrollably until it eventually becomes malign. This phenomenon can be identified based on different factors. In the report, the group will study the theory of if an algorithm can be trained to correctly detect and diagnose melanoma based on its asymmetry, color variability and the presence of a blue-white veil.

2 Data

2.1 Source

The PAD-UFES-20 dataset was created in collaboration with the Dermatological and Surgical Assistance Program (PAD) at the Federal University of Espírito Santo (UFES) in Brazil. This program offers free treatment for various skin lesions, focusing on those unable to afford private care. The dataset comprises 2,298 samples representing six distinct types of skin lesions. Each sample includes a clinical image and up to 22 clinical attributes, such as patient age, lesion location, Fitzpatrick skin type, and lesion diameter. Approximately 58% of the dataset's samples are biopsy-confirmed. The images in the dataset vary in size due to being captured by different smartphones and are stored in .png format. Metadata accompanying each lesion contains up to 26 features, available in a CSV file where each row represents a lesion and each column represents a metadata feature. Overall, the dataset comprises data from 1,373 patients, 1,641 skin lesions, and 2,298 images, with each image/sample linked to the corresponding patient and lesion in the metadata. Additionally, the group found that the images provided did not include enough features to conduct the tests mentioned later in the report. As such, more were imported from Dermoscopedia, the National Institutes of Health (NIH) and ResearchGate, which included more of the features that came to be studied. These images were used for the training of the classifiers.

2.2 Data Cleaning

Upon analysis, the images were classified into two distinct categories: low quality and high quality. Upon further examination, it was evident that within the Low quality subset, some images still retained identifiable lesions. Consequently, the Low quality category was subdivided into usable and unusable segments. Notably, four pictures from the data set were deemed unusable (`PAT_246_377_159.png; PAT_153_233_45.png; PAT_356_4511_960.png; PAT_1618_2771_628.png`) due to the quality being too low to identify any feature relevant for this report.

3 Methodology

3.1 Image Reduction

The images from the data set include a large area that is not relevant for this research. For this reason, the group conducted a process of segmentation masks to crop the image down to a thin frame around the identifiable lesions. Not only did this process allow for a more adequate identification of the RGB channels of the lesion, but also promoted a swifter process and run time overall.

3.2 Feature Extraction

The group created different functions in order to extract specific features from the images. The features chosen for the tests were based on the medical suggestions that high color variability, low symmetry and presence of blue-white veils could indicate melanoma. Additionally, these factors are relatively more evident to the human eye, when compared to the other possibilities, which contributed to the decision of the group for which features to work with.

Color: This code loads an image and its corresponding mask, calculates the variance of colors within the lesion area defined by the mask, based in the RGB values. Then, it computes a color score based on the sum of variances across all color channels. Finally, it categorizes the score into the ascending levels of 1, 2, 3 or 4. HSV test was also considered, however its methodology is based on the intensity of each color, which the human eye cannot evaluate as easily, thus making non-viable for a comparison between the computer test and the human test. Additionally, it also proved to not be as efficient for the data as the RGB test, as shown on Figure 1 and Figure 2.

Symmetry: The code use here computes the symmetry score of a lesion based on its shape and orientation. It starts by doubling the size of the input image with a black background, so that while rotating around the longest diameter it would not be outside of the image borders, then, it finds the longest diameter of the lesion in the mask. It aligns the longest diameter vertically or horizontally, depending on its angle, by rotating the mask. Finally, it crops it to the minimum bounding box. After this, it calculates the pixel (sum of 0 or 1 entries of the mask) differences between the left and the right halves vertically and horizontally, determining the fraction of similarity for both cases. As a result, it places each score into, again, four ascending levels (1, 2, 3 or 4).

Blue-White Veil: For the third test, the objective is to identify the occurrence of a blue or white veil, which can be indicative of melanoma. The code converts the image to the HSV color space, and defines ranges for detecting blue and white colors in it. It creates masks for the blue and white colors separately. Then, it combines the to identify areas with a blue-white veil, and it calculates the ratio of its area to the area of the whole lesion. Finally, it returns a binary score where 1 represents the presence of a blue-white veil and 0 the absence.

3.3 Group Test

For all three of the above mentioned tests, the members of the group conducted an individual rating of each image into the same categories as the code did. The average of these results was used to compare the interpretation of the images by the human eye and by a computer.

3.4 Comparison between Computer and Human

For each of the tests, the results of the computer and the mean of the group members were compiled into plots. This mean is then approximated to its closest rating (1, 2, 3 or 4). If this value matches the computer test, it creates a ’yes’, otherwise, a ’no’.

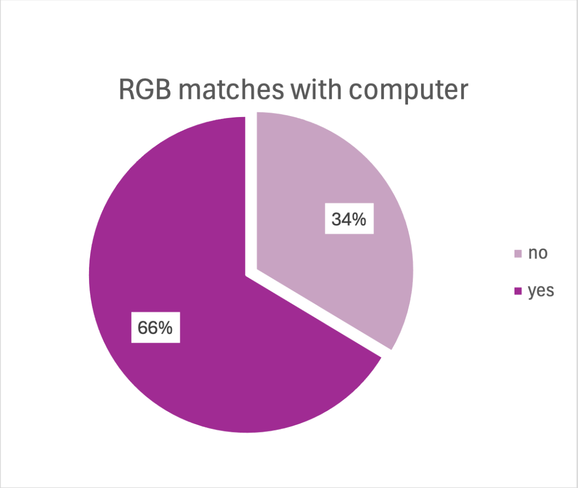

Figure 1: Matches between the computer and the human RGB tests

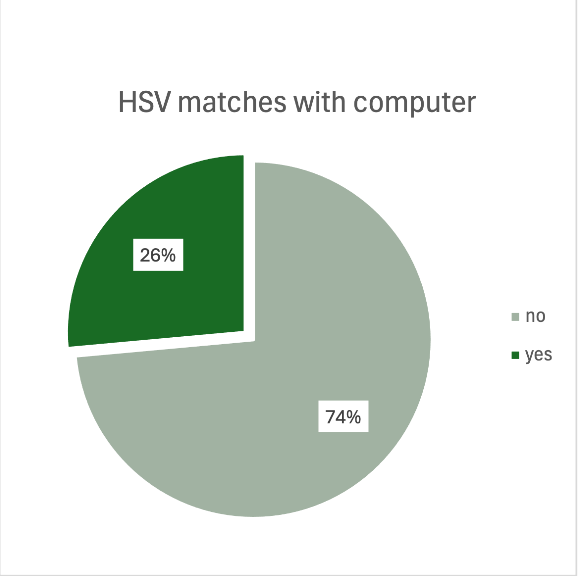

Figure 2: Matches between the computer and the human HSV tests

After analyzing both charts, the different inaccuracies of the RGB test (34%) and of the HSV test (74%) was the reason why the group chose to use only the RGB test for the remaining of the study.

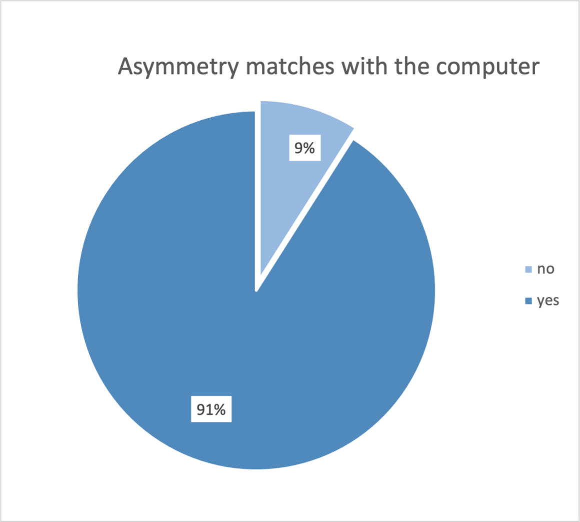

Figure 3: Matches between the computer and the human Asymmetry tests

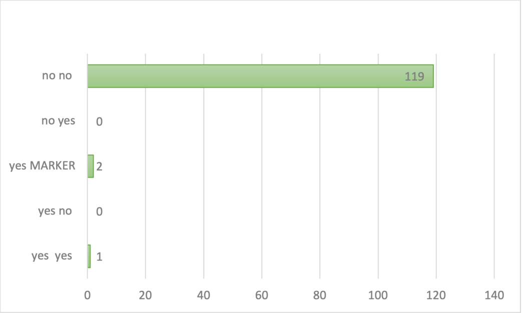

Figure 4: Matches between the computer and the human Blue-white veil tests

In this plot, the first bar shows the instances where the computer and the human tests both detected no blue-white veil. For the 'no yes' and 'yes no', it is shown that there are no cases of the computer not detecting but the human doing so, or vice-versa. The 'yes MARKER' proves that there two occurrences of the computer detecting a blue-white veil, but upon human inspection it was found that those were actually misinterpretations of blue dots made by a marker or a pen. The last bar shows the only instance of a blue-white veil detected by both the computer and the human tests.

There is an additional graph in the appendix (Figure 15), which shows that although there are some instances where the mean does not match the computer, which generates a "no" as represented in Figure 1 , the deviation is usually only one point in the scale. This proves that the level of inaccuracy, although being 34%, is not as big as the graph would suggest.

3.5 Diagnostic

The data set used for the report includes the actual diagnosis made by a biopsy to each lesion in the images. This diagnosis classifies each image by the type of legion in includes. The ones labeled with 'MEL' are melanoma, and represent a '1' for in the binary classification used for the project, while any other label represents a '0'.

3.6 Comparison between Computer and Diagnostics

TABLE

4 Machine Learning

4.1 Classifiers

The group conducted a wide variety of tests to find the best model to train to detect melanoma.

4.2 KNN

K-Nearest Neighbors (KNN) is a machine learning algorithm used for classification and regression tasks. It works by finding the K closest data points to a new observation and using them to predict its label or value. KNN is based on the principle that similar things tend to be near each other. The algorithm begins by importing necessary libraries and setting a random seed for reproducibility. It then loads data from a CSV file and splits it into features and labels. After that, it prints the class distribution. Subsequently, the data is divided into training and test sets. Following this, a pipeline is constructed for data preprocessing (standardization) and classification using KNN with specified hyper-parameters. The code proceeds to train the classifier on the training data and generates learning curves to visualize the model's performance.

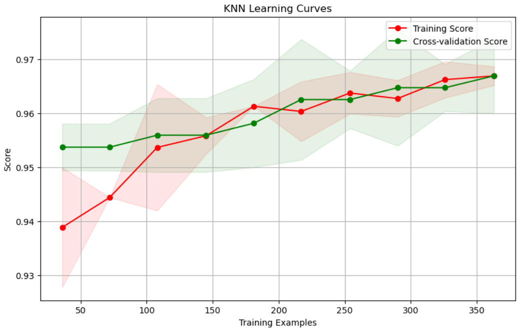

Figure 5: Learning curves for the KNN classifier

The algorithm then makes predictions on the test set, and further evaluation of the model's performance is conducted by generating a confusion matrix and classification report.

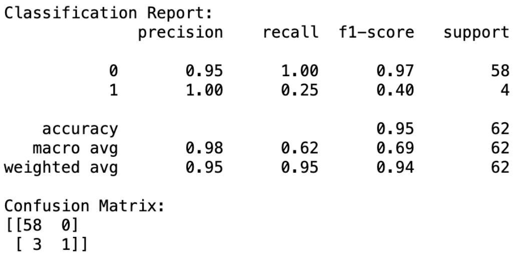

```
Classification Report:
              precision    recall  f1-score   support

           0       0.95      1.00      0.97        58
           1       1.00      0.25      0.40         4

    accuracy                           0.95        62
   macro avg       0.98      0.62      0.69        62
weighted avg       0.95      0.95      0.94        62

Confusion Matrix:
[[58  0]
 [ 3  1]]
```

Figure 6: Classification report and confusion matrix for the KNN classifier

4.3 Decision Tree

The decision tree model partitions the data based on features, aiming to maximize the information gain or minimize impurity at each step. As a result, it creates a hierarchical structure of decisions, with each node representing a decision based on a feature and each leaf node representing a class label. The code starts by importing necessary libraries and setting a random seed for reproducibility. It then loads data from a CSV file and splits it into features and labels. Next, it prints the class distribution. The data is subsequently divided into training and test sets. After that, a pipeline is constructed for data pre-processing (standardization) and classification using a Decision Tree Classifier with specified hyper-parameters. The model proceeds to train the classifier on the training data, and it generates learning curves to visualize the model's performance.

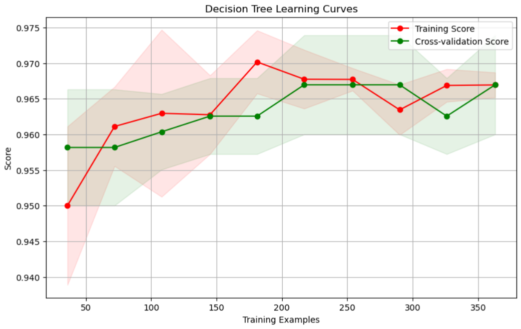

Figure 7: Learning curves for the Decision Tree classifier

Again, the algorithm makes predictions on the test set, and further evaluation of the model's performance is conducted by generating a confusion matrix and classification report.

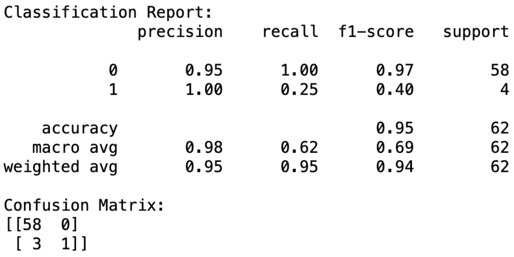

```
Classification Report:
              precision    recall  f1-score   support

           0       0.95      1.00      0.97        58
           1       1.00      0.25      0.40         4

    accuracy                           0.95        62
   macro avg       0.98      0.62      0.69        62
weighted avg       0.95      0.95      0.94        62

Confusion Matrix:
[[58  0]
 [ 3  1]]
```

Figure 8: Classification report and confusion matrix for the Decision Tree classifier

4.4 Random Forest

Random Forest is an algorithm that utilizes an ensemble of decision trees. Each tree is trained on a random subset of the data and features, promoting diversity and reducing over-fitting. This code performs a machine learning classification task using a Random Forest Classifier. It starts by importing necessary libraries and setting a random seed for reproducibility. Then, it loads data from a CSV file and divides it into features (X) and labels (y). It prints the class distribution of the labels. Next, the data is split into training and test sets. The code constructs a pipeline for data preprocessing (standardization) and classification using a Random Forest Classifier with specified hyperparameters. It then trains the classifier on the training data and generates learning curves to visualize the model's performance.

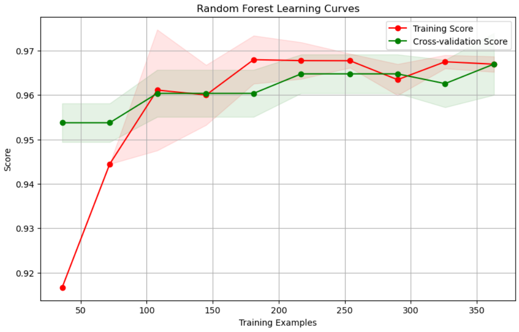

Figure 9: Learning curves for the Random Forest classifier

Mean and standard deviation of training and validation scores are calculated. Predictions are made on the test set, and further evaluation of the model's performance is conducted by generating a classification report and a confusion matrix.

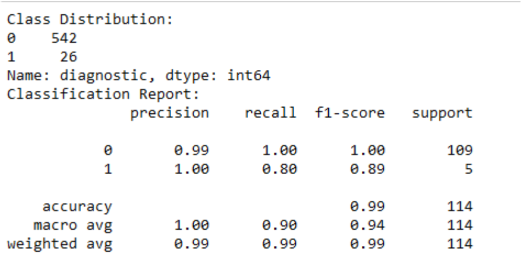

```
Class Distribution:
0    542
1     26
Name: diagnostic, dtype: int64
Classification Report:
              precision    recall  f1-score   support

           0       0.99      1.00      1.00       109
           1       1.00      0.80      0.89         5

    accuracy                           0.99       114
   macro avg       1.00      0.90      0.94       114
weighted avg       0.99      0.99      0.99       114
```

Figure 10: Classification report for the Decision Tree classifier

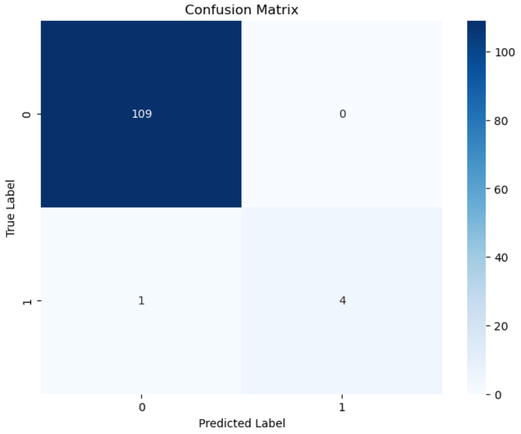

Figure 11: Confusion matrix for the Decision Tree classifier

4.5 Decision and Algorithm

After analysing the three options above mentioned, the group decided to use the Random Forest classifier to train an algorithm with the images from both data sets mentioned in section 2.1. This algorithm is meant to analyse images based on the factors Color variability, Symmetry and Presence of blue-white veil to conclude weather or not a lesion is melanoma, by comparing it with the results of a medical diagnose included on the data sets' descriptions.

5 Limitations

This research raised some questions along its conduction, regarding its accuracy and usefulness. Firstly, it is important to denote that the amount of images used to test and train each code was not enough to deem them safe and trustworthy. Not only did the images not offer a diverse enough set of lesions or skin tones and textures, a proper machine learning model requires a much more extensive training. Secondly, the way that the data was split for the machine learning algorithm could've caused a higher proportion of images with a blue-white veil on one of the pieces of data, which when dealing with such small quantities can cause large inaccuracies for the trained model. Lastly, the factors used for the project (color variability, asymmetry and presence of blue-white veil) are not enough to scientifically classify a lesion as melanoma or not. Although high color variability, high asymmetry and the presence of a blue-white veil indicate a higher likelihood of melanoma, it is not clear how the proportions of each factor actually affect the incidence. For instance, an image rated 4 on the RGB test, but 1 on the symmetry and 0 on the blue-white veil tests does not necessarily mean it is more or less likely than an image rated 1, 4 and 0, respectively. Therefore, it is important that the lesions undergo a biopsy to detect cancerous cells to be able to diagnose it as melanoma or not.

6 Open Question: Differences Between Groups of Patients Based on Age

6.1 Research Question

How do the visual features of skin lesions (color, symmetry and blue-white veil) differ between various age groups?

6.2 Motivation

Understanding the differences in skin lesion characteristics across different age groups can provide insights into how melanoma and other skin conditions manifest in patients of different ages. This can aid in better diagnostic approaches tailored to age-specific presentations of skin lesions.

6.3 Data and Methodology

The group analysed a dataset containing information about skin lesions, including visual features: color, symmetry and blue-white veil score. Then, divided the patients into five age groups: 0-20, 21-40, 41-60, 61-80, and 81-100. To determine if there are statistically significant differences in the visual features of skin lesions between these age groups, an ANOVA test was performed for each feature.

6.4 Results

1. Color Score

ANOVA Results: F-statistic: 0.480 p-value: 0.750

Interpretation: The high p-value (0.750) indicates that there is no statistically significant difference in the color scores between the different age groups. This suggests that age does not significantly influence the color variability of lesions.

2. Symmetry Score

ANOVA Results: F-statistic: 2.878 p-value: 0.026

Interpretation: The p-value (0.026) is less than 0.05, indicating a statistically significant difference in the symmetry scores between the different age groups. This suggests that the symmetry of lesions varies with age.

3. Blue-White Veil Score

ANOVA Results: F-statistic: 0.282 p-value: 0.889

Interpretation: The high p-value (0.889) indicates that there is no statistically significant difference in the blue-white veil scores between the different age groups. This suggests that age does not significantly influence the presence of a blue-white veil.

6.5 Visualizations

To further illustrate these findings, the group created bar plots showing the distribution of each score across the different age groups.

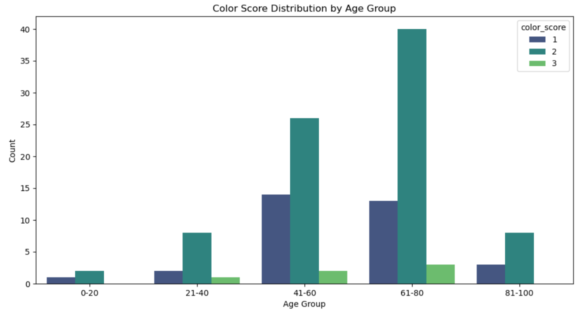

Figure 12: Color Score Distribution by Age Group

6.6 Conclusion

The findings indicate that while color score and blue-white veil score do not show significant differences across age groups, symmetry score does vary significantly with age. This could imply that as patients age, the symmetry of their skin lesions changes, which might be a relevant factor for dermatologists to consider during diagnosis. Further investigation through post-hoc tests can provide more granular insights into which specific age groups have significant differences in symmetry scores. Additionally, other factors such as gender, smoking, and drinking habits can be analyzed to see if they contribute to differences in lesion characteristics.

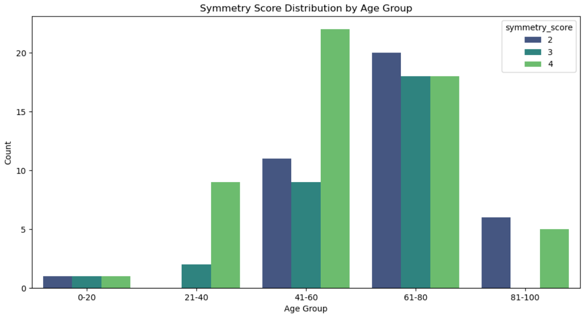

Figure 13: Symmetry Score Distribution by Age Group

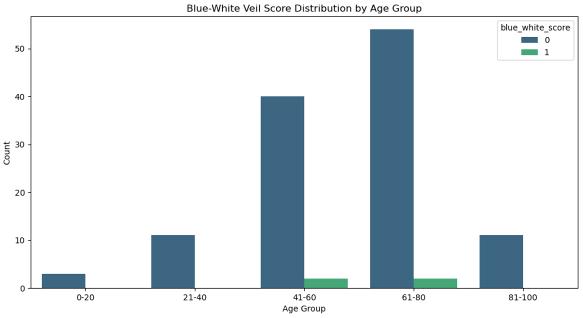

Figure 14: Blue-White Veil Score Distribution by Age Group

7 Summary and Recommendations

This report details the group's exploration of machine learning classification methods for melanoma detection, focusing on color variability, symmetry, and the presence of a blue-white veil in skin lesions. The code employs various techniques, including color variance calculation, symmetry analysis, and blue-white veil detection, to assess lesion characteristics. Human and computer interpretations of these features are compared, highlighting discrepancies and informing algorithm selection. After evaluating KNN, Decision Trees, and Random Forest classifiers, the group opts for Random Forest due to its superior performance. It is important to admit that this study is not complete, however. As it was explored in the open question, different factors such as age can affect these results. Additionally, the limitations for the research are extensive, and prevent the trained model to be used in any trustworthy medical way. Finally, a functioning trained model should still not be interpreted as a tool for a diagnose, but as a recommendation to further concern, which to be to visit a doctor and go under the proper medical routes to get a diagnose.

References

Andre G. C. Pacheco and Gustavo R. Lima and Amanda S. Salomão and Breno Krohling and Igor P. Biral and Gabriel G. de Angelo and Fábio C. R. Alves Jr and José G. M. Esgario and Alana C. Simora and Pedro B. C. Castro and Felipe B. Rodrigues and Patricia H. L. Frasson and Renato A. Krohling and Helder Knidel and Maria C. S. Santos and Rachel B. Espírito Santo and Telma L. S. G. Macedo and Tania R. P. Canuto and Luíz F. S. de Barros 2020. *PAD-UFES-20: a skin lesion dataset composed of patient data and clinical images collected from smartphones*. Mendeley Data, V1. doi:10.17632/zr7vgbcyr2.1.

A. Madooei and M.S. Drew and M. Sadeghi and M.S. Atkins 2013. Automatic detection of blue-white veil by discrete colour matching in dermoscopy images. *Med Image Comput Comput Assist Interv*, 16(Pt 3):453-60. doi:10.1007/978-3-642-40760-4_57. PMID:24505793.

Cancer.Net. 2023. *Melanoma*. Retrieved from https://www.cancer.net/cancer-types/melanoma/view-all (Accessed Oct. 9, 2023).

National Comprehensive Cancer Network. 2023. *Melanoma: Cutaneous*. Retrieved from https://www.nccn.org/guidelines/guidelines-detail?category=1&id=1492 (Accessed Oct. 9, 2023).

Niederhuber JE, et al., eds. 2020. *Melanoma. In: Abeloff's Clinical Oncology*. 6th ed. Elsevier. Retrieved from https://www.clinicalkey.com (Accessed Oct. 9, 2023).

National Cancer Institute. 2023. *Melanoma treatment (PDQ) – Patient version*. Retrieved from https://www.cancer.gov/types/skin/patient/melanoma-treatment-pdq (Accessed Oct. 9, 2023).

National Cancer Institute. 2023. *Common moles, dysplastic nevi and risk of melanoma*. Retrieved from https://www.cancer.gov/types/skin/moles-fact-sheet (Accessed Oct. 10, 2023).

Rashid S, et al. 2023. *Melanoma classification and management in the era of molecular medicine. Dermatology Clinics*, doi:10.1016/j.det.2022.07.017.

National Cancer Institute. 2023. *Sunlight*. Retrieved from https://www.cancer.gov/about-cancer/causes-prevention/risk/sunlight (Accessed Oct. 10, 2023).

Allan C. Halpern, MD; Ashfaq A. Marghoob, MD; Ofer Reiter, MD. 2021. *Melanoma Warning Signs: What You Need to Know About Early Signs of Skin Cancer*.

Oriol Yélamos. 2023. *Blue White Structures*.

Ali Madooei, Mark Drew, Maryam Sadeghi, Margaret Atkins. 2013. *Automatic Detection of Blue-White Veil by Discrete Colour Matching in Dermoscopy Images*. *Medical image computing and computer-assisted intervention : MICCAI ... International Conference on Medical Image Computing and Computer-Assisted Intervention*, volume 16, pages 453-60. ISBN: 978-3-642-38708-1. DOI: 10.1007/978-3-642-40760-457.

8 Appendix

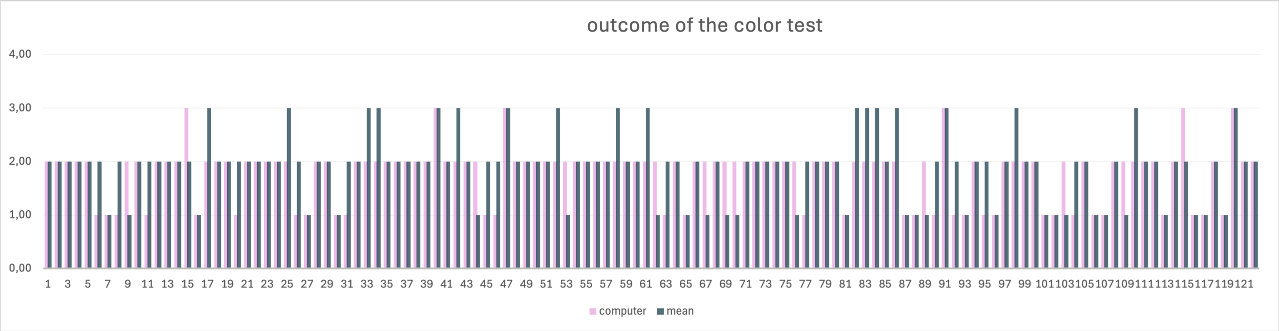

Figure 15: Outcome of the color test